Mechanical Vibration Sensing for Structural Health Monitoring Using a Millimeter-Wave Doppler Radar Sensor

Jochen Moll, Kaspar Bechtel, Bernd Hils, Viktor Krozer

MECHANICAL VIBRATION SENSING FOR STRUCTURAL HEALTH MONITORING USING A MILLIMETER-WAVE DOPPLER RADAR SENSOR

Jochen Moll, Kaspar Bechtel, Bernd Hils, Viktor Krozer

Goethe University of Frankfurt, Department of Physics, Terahertz Photonics Group, Max-von-Laue-Strasse 1, 60438 Frankfurt am Main, Germany, moll@physik.uni-frankfurt.de

ABSTRACT

In-service detection of material failures based on an integrated sensor network is the main goal of structural health monitoring (SHM). In this paper, we report on a millimeter-wave Doppler radar sensor operating at 102 GHz that enables accurate and non-contact mechanical vibration sensing. Thanks to the unique properties of mm-wave radiation it is possible to penetrate through many non-conducting materials. In contrast to Laser-Doppler-vibrometry this modality enables non-contact vibration measurements behind barriers such as glass-fiber-reinforced plastics, sandwich structures, foams, ceramics etc. Experimental measurements are shown for damage detection and non-linear motion sensing. The unique properties of mm-wave radiation promise great potential for a multitude of future SHM-applications.

KEYWORDS : *remote vibration sensing, millimeter-waves, structural health monitoring.*

INTRODUCTION

Structural health monitoring based on vibration measurements has a long tradition [1]. In these applications the mechanical vibrations are normally sensed via accelerometers, strain gauges or Laser-Doppler vibrometers. A different approach for measuring vibrations of large structures is given by radar interferometry. This refers to a remote sensing technique that is able to detect small deformations at large distances [2]. The working principle is based on two antennas arranged next to each other, with which the phase differences of the reflected electromagnetic radiation can be measured. A widespread usage for structural dynamics studies is limited by high equipment costs.

Subsequently, we will focus on millimeter-wave radiation that is part of the electromagnetic spectrum at frequencies between 30 and 300 GHz. This corresponds to a wavelength of 10 mm and 1 mm, respectively. Several interesting properties can be exploited for non-contact vibration sensing:

- The short wavelength enables mechanical oscillations measurements with small amplitudes.
- Vibration sensing is performed in a contactless way, similar to Laser-Doppler vibrometry, with good signal-to-noise ratio.
- Most non-conductive materials are transparent at these frequencies so that mechanical oscillations of buried objects can be detected.
- Millimeter waves propagate in dust and water vapor with low attenuation which enables large propagation distances (up to few kilometers).
- Electromagnetic radiation at typical power-densities is harmless for humans [3].
- They have a low sensitivity with respect to the surface state of the object being investigated.
- Radar modules can be manufactured on a low-cost basis (compare automotive industry).

Microwaves and millimeter-waves have been applied in many studies for non-contact respiration and heart beat sensing [4]. Since the electromagnetic waves are able to penetrate through rubbles it is possible to use this technique to search for buried people [5]. A major challenge, especially for vital sign measurements, are random body movements. To solve this problem, the detection can be performed from multiple sides or using a differential radar front-end operating at two different frequencies [6]. A terahertz sensor for measuring mechanical vibrations behind optically opaque materials has been proposed in [7]. The application of mm-wave vibration sensing for SHM purposes is new and only few papers have been published on that topic. An example is given by radar-based monitoring of a bridge in [8]. Furthermore, condition monitoring of a propulsion system has been reported in [9].

In recent years, millimeter-waves and submillimeter-waves up to 1000 GHz gain more and more attention in the Non-Destructive-Testing community to determine three-dimensional images of one or multiple defects [10]. The aim of this NDT-method consists in spatially resolved damage diagnostics, especially suited for damage detection in glass-fiber-reinforced plastics, sandwich structures, foams, ceramics, etc. For this purpose Synthetic Aperture Radar (SAR) methods are widely used [11, 12]. However, this NDT-method is limited when the material under test cannot be penetrated by the electromagnetic waves, e.g. in the case of carbon fiber reinforced plastics [13].

On one hand, the contribution of this paper is to demonstrate the ability of using millimeter-waves for measuring mechanical vibrations behind barriers that are transparent at mm-wave frequencies. On the other hand, it will be shown that the measured time-series can be used for the assessment of structural defects. Therefore, Section 1 presents the underlying theory of a Doppler radar sensor and the complex arctan-demodulation of I-Q-signals. After that, Section 2 introduces the experimental setup used in this study in conjunction with measurement results of linear and non-linear motion.

1. THEORY

There are different mechanisms for motion sensing radars that are summarized in [6], i.e. Doppler frequency shift, Doppler nonlinear phase modulation, pulse radar and FMCW radar. In this paper, we will consider a radar system that exploits the Doppler frequency shift. Hence, the following section starts with a brief description of the underlying theory.

1.1 Signal Model of a Doppler Radar System

In conventional Doppler radars the transmitter emits a continuous wave signal $s(t)$ at the frequency f_0 with the residual phase $\phi_1(t)$ [6]. That signal is given by

$$T(t) = \cos\left(2\pi f_0 t + \phi_1\right). \tag{1}$$

When the target is moving with a velocity v along the line-of-sight of the radar, as shown in Fig. 1, then a Doppler frequency shift occurs that is measured by the radar receiver. The plus sign in the following equation corresponds to a motion in the direction of the antenna, while a negative sign denotes a motion in the reverse direction. The received signal can be described as

$$R(t) = \cos\left(2\pi f_0 t \pm \frac{4\pi v t}{\lambda} + \phi_2\right), \tag{2}$$

where the phase term changes to ϕ_2 due to additional phase noise and variation of the nominal measurement distance. The Doppler frequency can be expressed as

$$f_D = \frac{2 v f_0}{c}, \tag{3}$$

using the relationship $c = \lambda f_0$. Consequently, the frequency of the received signal is given by $f_0 \pm f_D$. After downconversion to base-band the resulting output signal is given by $R_B(t) = \cos(\pm 2\pi f_D t + \Delta\Phi)$.

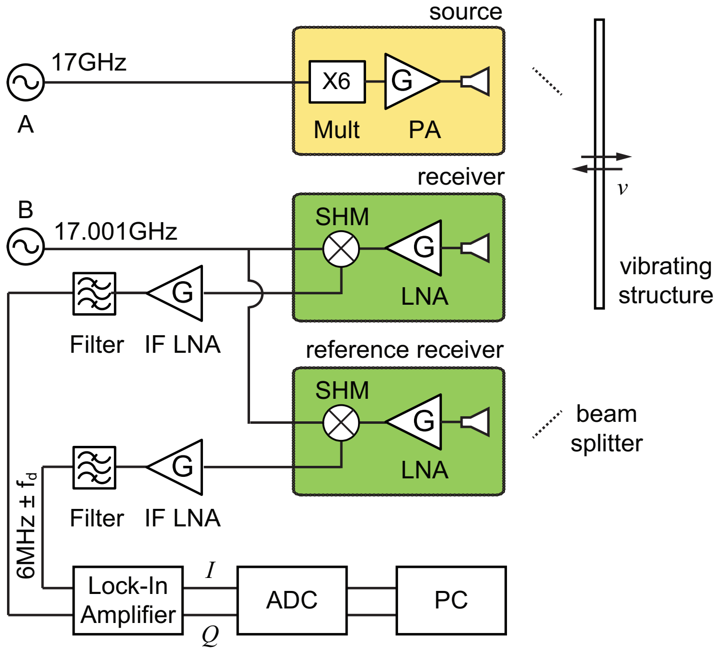

Figure 1 : Flowchart of the mm-wave Doppler heterodyne radar sensor.

1.2 Complex Signal Demodulation

Since a typical quadrature radar has two channels, I (in-phase) and Q (quadrature), complex signal demodulation needs to be performed in base-band. In many cases the well-known arctangent demodulation is used. For a proper determination of amplitude and phase, the Doppler radar requires accurate DC calibration due to a lack of quadrature of the I-Q-signal [14]. This procedure centers the constellation diagram at its origin. The phase function is given by

$$\varphi(t) = \arctan \frac{Q(t)}{I(t)} + H, \tag{4}$$

where $I(t)$ and $Q(t)$ denote the time-dependent I- and Q-channel, respectively. Furthermore, H stands for a phase correction term when the jumps in the phase function are larger than π. This procedure is called phase-unwrapping. Consequently, the amplitude relation is given by

$$R(t) = \sqrt{Q(t)^2 + I(t)^2}. \tag{5}$$

There is a direct relationship between $\varphi(t)$ and the displacement $x(t)$ given by Equation (6). In this expression, k denotes the wave-number in free space and λ the wavelength. Here, $x(t)$ must be divided by 2 to account for the two-way propagation.

$$x(t) = \frac{1}{2}\frac{\varphi(t)}{k} = \frac{1}{2}\frac{\varphi(t)\lambda}{2\pi}. \tag{6}$$

2. Results

2.1 Experimental Setup

The experimental setup proposed in this paper is a full-electronic implementation of the system described in [15]. A schematic of the radar setup is shown in Fig. 1 and the corresponding experimental

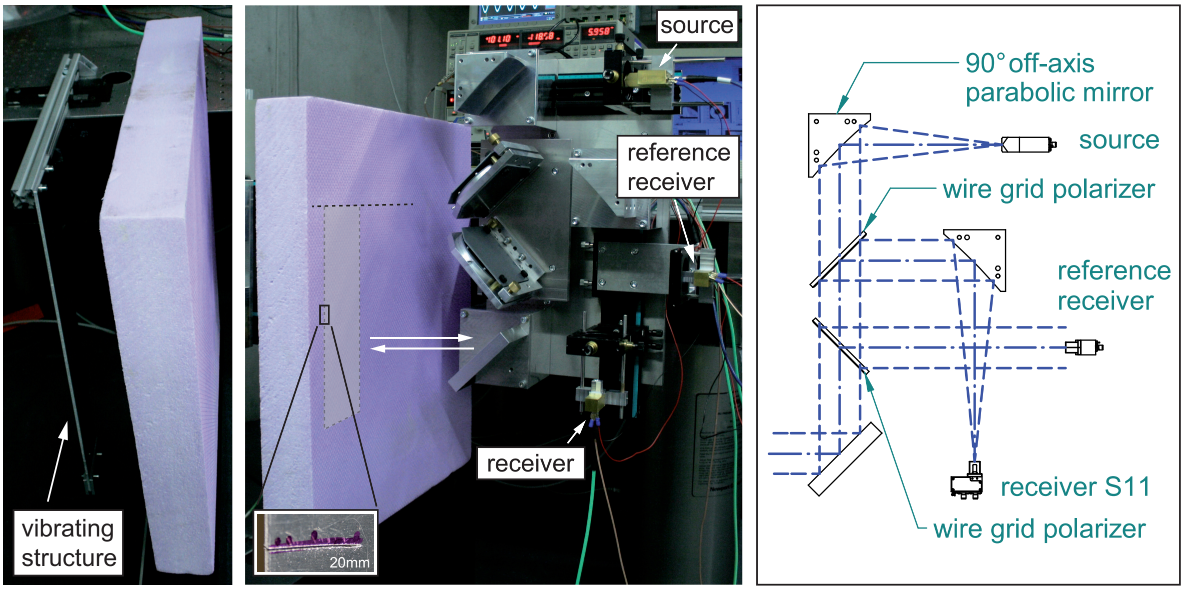

Figure 2 : (left) Experimental setup for mm-wave remote sensing; submillimeter-vibrations are found behind a barrier of 80mm thick polystyrene foam; (right) Millimeter-wave path within the experimental setup.

realization in Fig. 2. Two synthesizers, indicated by A and B, have been used to generate continuous wave signals of 17 GHz and 17.001 GHz, respectively. The former signal for the transmitter is forwarded to a frequency multiplier that multiplies the frequency of the signal by a factor of six. Consequently, the signal transmitted by the diagonal horn antenna has a frequency of 102 GHz which corresponds to a wavelength of $\lambda \approx 3mm$.

The right part of Fig. 1 illustrates the structure oscillating with the velocity v. The direct signal from the transmitting antenna is recorded by the reference receiver to provide the reference signal. The reflections from the vibrating structure are measured by the receiving antenna. Detuning the synthesizers by 1 MHz in combination with subsequent frequency multiplication leads to an intermediate frequency (IF) of 6 MHz. It is worth noting that the IF can be defined in a certain frequency range depending on the filter properties of the W-band receivers. For practical reasons we have defined the IF as 6 MHz. The lock-in amplifier demodulates the I- and Q-signals which are sampled with 20 kHz for further data analysis.

As shown in Fig. 2 we have placed a barrier of 80mm thick polystyrene foam between the antenna and the beam structure. The intention is to demonstrate the unique properties of mm-waves to penetrate through this non-conducting material. Such an experiment cannot be performed with a conventional Laser-Doppler-vibrometer since the laser beam cannot pass that barrier material. The path of the millimeter-waves within the experimental setup is presented in the right part of Fig. 2. A collimated beam is sent towards the structure under test. Various experiments have been conducted with the proposed setup as outlined below. In each experiment an impulse excitation by a hammer has been used where the impact point is 200 mm from the bottom of the structure.

2.2 The Barrier Effect

Fig. 3(a) shows a basic comparison using the displacements measured with and without the barrier. The impact has been performed manually so that there is a difference in impact time and amplitude leading to a lack of coherence in the excitation signal. Note that the unwrapped phase and hence the displacements have not been filtered. This demonstrates the excellent signal to noise ratio (SNR). A constant increase of the optical path difference occurs due to the difference of the refractive indices

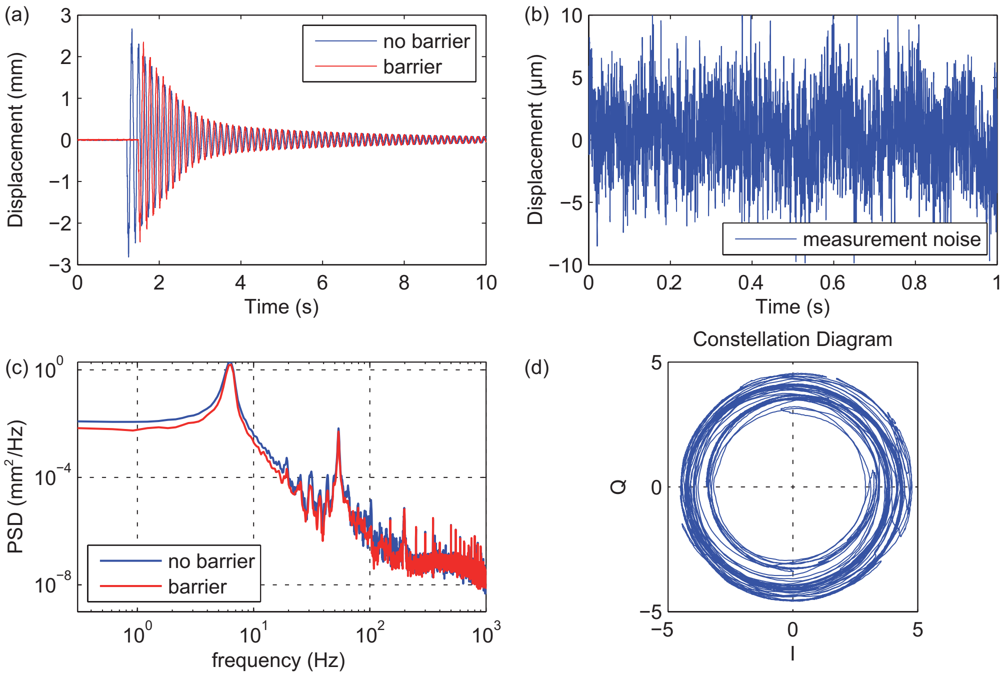

Figure 3 : (a) Displacement for barrier / no barrier (unfiltered); (b) close-up of the displacement to show the measurement noise; (c) Comparison of power spectral densities; (d) centred constellation diagram.

between air and foam. However, this phase shift has no influence on the dynamics measurements as demonstrated in Fig. 3(a).

Fig. 3(b) illustrates a close-up of the displacement measurement indicating that the amplitudes of the measurement noise are $< 10\ \mu m$. In a next step, power spectral densities (PSD) have been calculated based on Welch's method. The results are illustrated in Fig. 3(c) showing a good agreement for both cases. It is also interesting to note that not only the fundamental, but also the higher order vibration modes can be measured. The phase demodulation requires DC-calibration that leads to the centered constellation diagram in Fig. 3(d).

2.3 Damage Detection

The proposed setup has been used to detect structural defects behind a polystyrene foam. Therefore, Fig. 4(a) shows the displacement measurements for the pristine structure and the structure having a crack of 20mm. The corresponding PSDs are shown in Fig. 4(b). A good agreement can be found between repeating measurements for both scenarios, proving the reliability of the measurements. And, as expected, the eigenfrequency of the fundamental and higher order modes are shifted to lower frequencies due to a lower stiffness of the damaged structure. By means of this simple case study we are able to demonstrate the proof-of-principle for millimeter-wave sensing for structural monitoring.

2.4 Nonlinear Motion Sensing

In the final experiment, we have investigated the possibility to measure nonlinear motion. Therefore, the excited structure hits a massive block that limits its motion in one direction. Note that the displacement in positive direction is constraint as a result of the blocking mass. The close-up in Fig. 5(a) shows that after approximately 1.5 s the structure vibrates freely. The non-linear motion is studied via time-frequency analysis using a Short-Time-Fourier-Transform in Fig. 5(b).

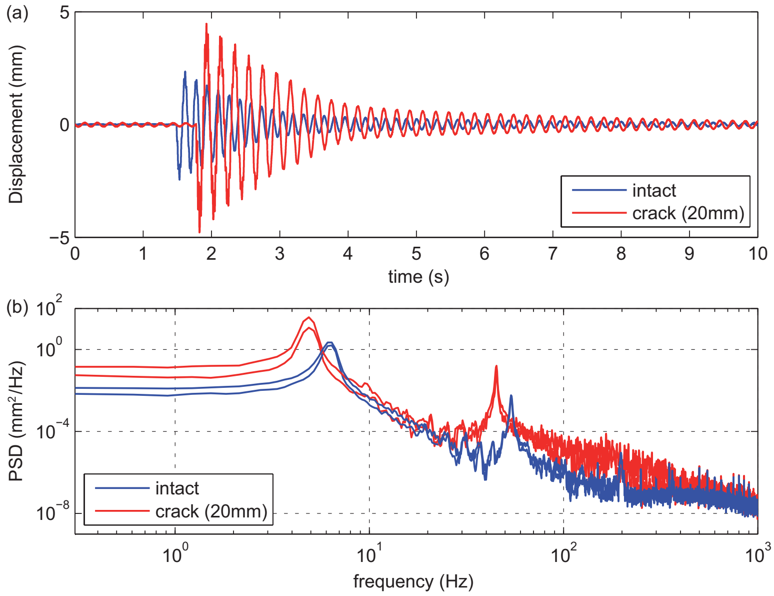

Figure 4 : (a) Displacement measurements (b) Power spectral densities for the intact and the damaged structure (two measurements for each case).

CONCLUSIONS

In this paper, we have demonstrated the potential of millimeter-wave sensing of mechanical vibrations for the purpose of structural health monitoring. In contrast to existing sensor technologies mm-waves penetrate through many non-conducting materials so that vibration measurements of hidden objects can be obtained in a non-contact way. In the future, this will lead to many interesting new SHM-applications, especially when multiple transmitter and receivers in a MIMO-setup will be used.

REFERENCES

[1] W. M. Ostachowicz and Alfredo Guemes, editors. *New trends in structural health monitoring*. Number volume 542 in CISM International Centre for Mechanical Sciences: courses and lectures. Springer, Wien ; London, 2013.

[2] Massimiliano Pieraccini. Monitoring of civil infrastructures by interferometric radar: A review. *The Scientific World Journal*, 2013:1–8, 2013.

[3] Guidelines for limiting exposure to time-varying electric, magnetic, and electromagnetic fields (up to 300 GHz). International Commission on Non-Ionizing Radiation Protection. *Health physics*, 74(4):494–522, April 1998. PMID: 9525427.

[4] Changzhi Li, Victor M. Lubecke, Olga Boric-Lubecke, and Jenshan Lin. A review on recent advances in doppler radar sensors for noncontact healthcare monitoring. *IEEE Transactions on Microwave Theory and Techniques*, 61(5):2046–2060, May 2013.

[5] Kun-Mu Chen, Yong Huang, Jianping Zhang, and A. Norman. Microwave life-detection systems for searching human subjects under earthquake rubble or behind barrier. *IEEE Transactions on Biomedical Engineering*, 47(1):105–114, January 2000.

[6] Changzhi Li. *Microwave noncontact motion sensing and analysis*. John Wiley & Sons Inc, Hoboken, New Jersey, 2013.

[7] Jerry C. Chen and Sumanth Kaushik. Terahertz interferometer that senses vibrations behind barriers. *IEEE Photonics Technology Letters*, 19(7):486–488, 2007.

[8] Shanyue Guan, Jennifer A. Rice, Changzhi Li, and Changzhan Gu. Simulation analysis and experimental performance of a radar sensor network for distributed bridge monitoring. page 869215, April 2013.

[9] Mark Woike, Ali Abdul-Aziz, Nikunj Oza, and Bryan Matthews. New sensors and techniques for the structural health monitoring of propulsion systems. *The Scientific World Journal*, 2013:1–10, 2013.

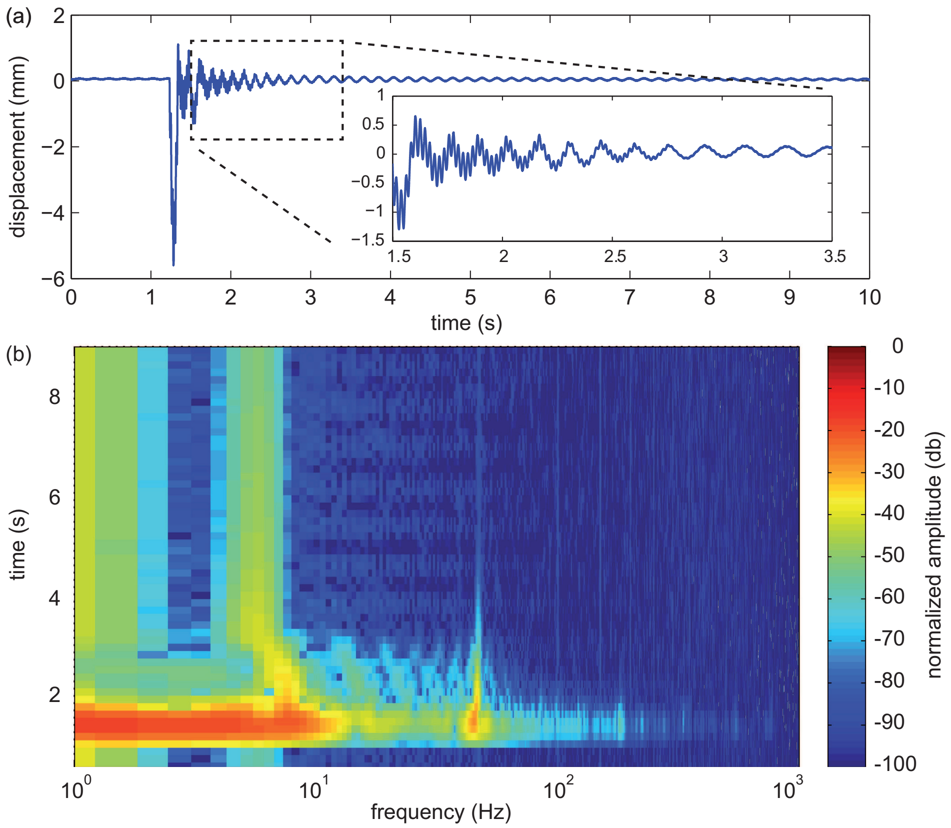

Figure 5 : (a) Displacement of the nonlinear motion experiment (b) Short-Time-Fourier-Transform of the displacement signal.

[10] Sergey Kharkovsky and Reza Zoughi. Microwave and millimeter wave nondestructive testing and evaluation - overview and recent advances. *IEEE Instrumentation & Measurement Magazine*, 10(2):26–38, April 2007.

[11] Anna Brook, Edison Cristofani, Mathias Becquaert, Ben Lauwens, Joachim Jonuscheit, and Marijke Vandewal. Applicability of compressive sensing on three-dimensional terahertz imagery for in-depth object defect detection and recognition using a dedicated semisupervised image processing methodology. *Journal of Electronic Imaging*, 22(2):021004, 2013.

[12] Jochen Moll, Viktor Krozer, Ralph Zimmermann, Bjrn Rolef, Timo Jaeschke, Nils Pohl, and Rahmi Salman. Luggage scanning at 80 GHz for harbor environments. In *European Conference on Synthetic Aperture Radar (EUSAR), accepted*, 2014.

[13] David Kuei Hsu, Kil-Sung Lee, Je-Woong Park, Yong-Deuck Woo, and Kwang-Hee Im. NDE inspection of terahertz waves in wind turbine composites. *International Journal of Precision Engineering and Manufacturing*, 13(7):1183–1189, July 2012.

[14] Peter L. M. Heydemann. Determination and correction of quadrature fringe measurement errors in interferometers. *Applied Optics*, 20(19):3382, October 1981.

[15] Bernhard Hils, Mark D. Thomson, Torsten Loeffler, Wolff von Spiegel, Christian am Weg, Hartmut G. Roskos, Peter de Maagt, Dominic Doyle, and Ralf D. Geckeler. Terahertz profilometry at 600 GHz with 0.5um depth resolution. *Optics Express*, 16(15):11289, July 2008.